

Chandra Observations of Extended X-ray Emission in Arp 220

J.C. McDowell

Harvard-Smithsonian Centre for Astrophysics, 60 Garden Street, Cambridge, MA 02138,
USA

`jcm@cfa.harvard.edu`

D.L. Clements

Physics Dept., Imperial College, Prince Consort Road, London SW7 2BW, UK

`d.clements@ic.ac.uk`

S.A. Lamb

Center for Theoretical Astrophysics, Departments of Physics and Astronomy, Loomis
Laboratory, University of Illinois, 1110 W. Green Street, Urbana, IL 61801, USA

S. Shaked

University of Arizona, Dept. Astronomy, 933 North Cherry Avenue, Tucson, AZ
85721-0065, USA

N.C. Hearn

Center for Theoretical Astrophysics, Department of Physics, Loomis Laboratory,
University of Illinois, 1110 W. Green Street, Urbana, IL 61801, USA

L. Colina

Instituto de Estructura de la Materia (CSIC), Serrano 121, 28006 Madrid, Spain

C. Mundell

ARI, Liverpool John Moores University, Twelve Quays House, Egerton Warf, Birkenhead,
Wirral, Cheshire, CH41 1LD, UK

K. Borne

Raytheon Information Technology and Sciences Services, NASA Goddard Space Flight
Centre, Greenbelt, MD 20771, USA

A.C. Baker

Dept. Physics and Astronomy, Cardiff University, PO Box 913, Cardiff, CF24 3YB, UK

S. Arribas

Space Telescope Science Institute, ESA Space Telescope Division, 3700 San Martin Drive,
Baltimore, MD 21218

Received _____; accepted _____

ABSTRACT

We resolve the extended X-ray emission from the prototypical ultraluminous infrared galaxy Arp 220. Extended, faint edge-brightened, soft X-ray lobes outside the optical galaxy are observed to a distance of 10 to 15 kpc on each side of the nuclear region. Bright plumes inside the optical isophotes coincide with the optical line emission and extend 11 kpc from end to end across the nucleus. The data for the plumes cannot be fit by a single temperature plasma, and display a range of temperatures from 0.2 to 1 keV. The plumes emerge from bright, diffuse circumnuclear emission in the inner 3 kpc centered on the $H\alpha$ peak, which is displaced from the radio nuclei. There is a close morphological correspondence between the $H\alpha$ and soft X-ray emission on all spatial scales. We interpret the plumes as a starburst-driven superwind, and discuss two interpretations of the emission from the lobes in the context of simulations of the merger dynamics of Arp 220.

Subject headings: galaxies: starburst — galaxies: individual (Arp 220) — X-Rays: galaxies

1. Introduction

The evolutionary importance of energetic events on galactic scales has become central to our present understanding of cosmological evolution. The realization in the IRAS era (e.g. Soifer et al. 1984) that super-starburst ultraluminous infrared galaxies rivalled quasars in their energy output made it clear that for at least a subset of galaxies a large fraction of their stellar content and gas mass is drastically rearranged during interactions which last

from 10^8 to 10^9 years (Clements et al. 1996) The observation of superwinds (Chevalier & Clegg 1985) emphasizes the role of energetic events in galaxies in redistributing material both within a galaxy and into the intergalactic medium. The energy and momentum involved in the biggest train wrecks in the universe are released in a number of different channels: stellar velocity dispersions, tidal disruption, gas heating, mechanical energy deposited in the gas and stars, shock-triggered star formation and subsequent infrared emission.

Truman H. Safford (1836-1901) discovered the nebula Safford 7 (IC 1127) at Chicago on 1866 May 4 (Safford 1887), but recorded its position with an RA off by one minute of time. Javelle¹ (1905) rediscovered it as Javelle 1368 at Nice on 1903 Jul 25. It was recorded by Dreyer in IC2 (Dreyer 1910) as IC 4553, but the object remained obscure until A.G Wilson identified it on Palomar Sky Survey prints as unusual and Arp (1966) included it in his catalog of peculiar galaxies as Arp 220, the designation by which it is most commonly known today. The discovery of strong OH maser emission (Baan, Wood & Haschick 1982) and ultra-luminous far infrared output (Soifer et al. 1984) established Arp 220 as the prototypical infrared superluminous merger. ISO observations (e.g. Genzel et al. 1998, Lutz et al. 1998) support a starburst interpretation for the bulk of the luminosity and Scoville et al. (1998) locate a number of massive star clusters in the nuclear region using NICMOS. At a distance of 76 Mpc ($z= 0.018$; Kim & Sanders 1998), it is one of the most luminous objects in the local universe. The galaxy, with an apparent B magnitude of 13.9 and a total infrared luminosity (10-100 microns) of $1.5 \times 10^{12} L_{\odot}$, is believed to have been formed by the almost face-on collision of two spiral disks.

¹Stephane Javelle (1864-1917) is most famous for claiming to have seen a strange light on Mars, and appears thinly disguised in H.G. Wells' *War of the Worlds* (1898) as 'Lavelle of Java'.

In the optical, Arp 220 appears irregular and dusty, but other wavebands have been used to probe into the center of the object and reveal the presence of activity within a few parsecs of the nucleus. VLBI observations of Arp 220 suggest that the peak of the OH emission originates in a structure $\lesssim 1$ pc across (Lonsdale et al. 1994) and Rieke et al. (1985) claimed that as much as half of the luminosity in Arp 220 may be due to an active nucleus. Armus et al. (1995) used near-infrared spectra to suggest that as much as 80-90% of the total luminosity is powered by an obscured AGN. Dudley and Wynn-Williams (1997) use the depth of the silicate absorption feature to estimate a size for the emission region at 10 microns of only a few parsecs.

Eales & Arnaud (1988) reported the first detection of X-rays from Arp 220, using the Einstein IPC. However, their observation was confused by emission from a neighbouring group of galaxies first noted by Heckman et al. (1996) who carried out the first detailed study of the X-ray properties of the galaxy with the ROSAT PSPC. Their data show that the X-ray emission in the 0.1-2.4 keV band has a size of $\sim 30 \times 11$ kpc and a luminosity of between 4.3×10^{40} and 2.3×10^{41} ergs s $^{-1}$ and set an upper limit of $\sim 20\%$ of the observed X-ray emission associated with any single point source. They noted that the spatial extent of the X-ray emission was around 22 kpc, much larger than the IR-emitting region, and that the X-ray luminosity was an order of magnitude larger than that of normal spiral galaxies. The "double-bubble" morphology seen in optical emission-line images (Heckman, Armus & Miley 1987) coincided with the X-ray nebula seen with ROSAT, but the spatial resolution of those data was insufficient for a detailed comparison. Heckman et al. suggested that both the X-ray and line emission is due to a bipolar "superwind" driven out from the nucleus by a starburst or a dust-shrouded QSO. Gallagher et al (2002) report similar extended X-ray emission in the ultraluminous galaxy Markarian 231, although at $z=0.042$ the spatial resolution of their Chandra image reveals less detail than the observations presented here.

2. Observations and Data Analysis

We observed Arp 220 on 2000 Jun 24 for 56 ks with the ACIS camera on the Chandra X-ray Observatory as part of the Cycle 1 guest observer program. Arp 220 was placed on the S3 back illuminated chip near the node 0/node 1 boundary. Here we report on the extended emission from Arp 220; Clements et al (2002, Paper I) discuss the point sources in the nuclear region. Data reduction was carried out with CIAO version 2.1 and 2.2. The data were taken with the chip at a temperature of -120C and were gain-corrected using the revised file `acisD2000-01-29gainN0003.fits` from the July 2001 recalibration, which improves the calibration at low energies. The observation was relatively unaffected by background flares and only a small amount of exposure was removed, leaving an effective exposure time of 55756s. Astrometry was corrected using a revised geometry file (`telD1999-07-23geomN0004.fits`) which is believed to provide positions across the full ACIS field accurate to about 1 arcsecond.

The extended emission from Arp 220 is clearly visible in the raw data. The west lobe is dithered partly across the node 0 boundary, but the remainder of the emission is all on node 1. We generated spectral responses making use of the recently recalibrated (`acisD2000-01-29fef_piN0002.fits`) low energy response, both using the standard CIAO `mkrmf` tool and using the `calcrmf` tool developed by Alexey Vikhlinin (available from the Chandra software swap page), which produces a count-weighted average of the response. As expected, there was very little difference in the results from the two methods.

For global images, we used the background event files developed by Markevitch et al (2000), together with the standard exposure map tools, to generate background-subtracted, exposure corrected images in various energy bands. These corrected images were then normalized to retain the same mean number of counts, and adaptively smoothed using the `csmooth` program. X-ray color images of the smoothed data (Figs. 1 to 4) show

the morphology of the region and allow regions of different spectral properties to be distinguished. The smoothed images were used in further analysis only to define extraction regions, not to determine any numerical quantities.

For spectral studies we extracted PI count histograms for various regions in the emission (Fig. 5). We made two background spectra, one using the Markevitch background files and one using a local background extracted from two 50-arcsecond-radius circles at either end of node 1 in our dataset and containing 10650 counts. The two spectra were similar, and the results presented here use the local background. The galactic extinction in the direction of Arp 220 has a column of $4.1 \times 10^{20} \text{cm}^{-2}$ (Stark et al. 1992) and this has been used as a lower limit in our spectral fits.

3. X-ray emission from Arp 220

3.1. Overall morphology

The Chandra view of Arp 220 reveals structure on scales from one arcsecond to several arcminutes. We can distinguish four scales of interest: the nuclear region, the galaxy with two regions of extended emission (‘plumes’), the extended 20-kpc scale emission (‘lobes’), and the unrelated group of galaxies to the south reported by Heckman et al. (1996). The position angles of the plumes and lobes are in agreement with the PSPC and HRI structures described by Heckman et al. Here we describe the observations, leaving most physical interpretation to later sections.

The integrated spectrum from Arp 220 can be fit by the sum of several thermal contributions and a power law, and gives good agreement on the total flux with the individual fits to components, with 1694 net counts and a luminosity of $1.2 \times 10^{41} \text{erg s}^{-1}$, in good agreement with the estimates of Heckman et al (1996). The data on individual

components are summarized in Table 1 and discussed below.

3.2. The circumnuclear region

In the nuclear region we see hard emission on a scale of two to three arcseconds, and indications of bright point sources, denoted X-1 and X-4 in Paper I (Clements et al. 2002) close to the nucleus. A soft emission peak, denoted X-3 in Paper I, is also present and is extended over a diameter of 2.5 kpc. Its centroid is displaced 1.5 arcseconds to the northwest of the hard emission. The hard emission coincides with a dust lane in the galaxy (Joy et al. 1986), and indeed the soft emission is suppressed there. However, the absence of hard emission away from the nucleus shows that the spectral change is due to a different type of source, and not merely an absorption effect. In Paper I we presented reconstructed images and spectral fits to the nuclear sources X-1 to X-4.

3.3. The plumes

On a scale of a few kiloparsecs, we see two regions of bright extended X-ray emission, one on either side of the nucleus, along a position angle of 135-150 degrees. This emission was seen in the HRI observations reported by Heckman et al. (1996); we will refer to these regions as the NW and SE ‘plumes’. We cannot rule out that the emission comes from unresolved point sources, but if the plumes are two unrelated starburst regions we would expect binaries to contribute a hard component to the spectrum. Fig. 6 shows a contour plot of the reconstructed image of the plume region.

The bright region of the NW plume is about 3 kpc in extent and the SE plume is larger and brighter, 3 x 5 kpc in extent; the projected tip-to-tip length of the emission is 10 kpc. Each of the plumes appears to be roughly round, but with an elongation in the radial

direction for the SE plume. The emission is not sharp-edged, and the dimensions given here correspond to a contour of 10 percent of the peak surface brightness.

The east plume spectrum is inconsistent with that from a single temperature plasma. It includes a soft thermal contribution with a temperature of less than 0.25 keV, together with hotter thermal plasma or bremsstrahlung ranging from 1 to 5 keV. There are fewer counts in the west plume, but the spectrum definitely contains flux out to 2 keV. Formally, the data provides only an upper limit to the absorption column in the plumes of $1.5 \times 10^{22} \text{cm}^{-2}$. The difference in inferred intrinsic luminosity (source side of absorption) between assuming only foreground absorption and using this upper limit renders estimates of the unabsorbed luminosity for this soft emission uncertain by a factor of a thousand; the values in Table 1 should therefore be considered illustrative. The overall morphology of the plumes could also be affected by patchy absorption in the galaxy, but the visible dust lanes do not correlate with the plume boundaries except in the inner edge of the east plume. Radio observations (Hibbard, Vacca and Yun 2000) show the presence of an elongated HI emission feature to the NE and SW of the galaxy on 20 kpc scales; notably, the HI emission avoids the regions of X-ray emission - there is a gap in the HI which corresponds to the area with the plumes and is aligned with them. However, the measured column of the HI, less than $5 \times 10^{19} \text{cm}^{-2}$ in the region of the plumes, would provide too little absorption to affect the observed soft X-ray morphology. We will assume in the later discussion that the observed morphology corresponds to the actual distribution of soft X-ray emitting gas.

3.4. The lobes

Beyond the plumes we observe large, lower surface brightness extended oval regions (which we will refer to as the E and W ‘lobes’) which lie along a position angle of 100-110 degrees. This larger scale emission extends across 25 kpc from the end of one lobe to that

of the other, and each oval lobe is 8 kpc along its major axis. The east lobe has a major axis diameter of 23 arcseconds (8 kpc) along PA 90 degrees, and a minor axis diameter of 15 arcseconds (5 kpc). The west lobe is elongated NE to SW and may consist of two separate components; it is 10 x 22 arcseconds in size. We have estimated nominal centers of the east and west lobes at 11 and 8 kpc from the nucleus.

The smoothed image makes it appear that the lobes are edge brightened, although this is only marginally evident in the raw data and one might worry that it is an artifact of the smoothing process. Extracting counts from raw data in the lobe centers and the lobe rims shows a difference of 4 sigma, with 6 total counts in the 0.2-2 keV range for a pair of 5 arcsecond diameter circles in the E and W holes (lobe centers) respectively, compared to 26 total counts in a bright rim region of equal size. We conclude that the lobes are indeed edge-brightened, although an exposure three times as deep would provide a firm confirmation.

The lobes show marginal evidence for some very soft photons below 0.25 keV, but the spectral calibration of ACIS is still unreliable in that energy band. The spectrum is consistent with no absorption in excess of the foreground value from Stark et al.; formally, the best fits of the east lobe data to a two temperature Raymond-Smith model are with a lower temperature of 0.3 ± 0.1 keV and a higher temperature of 1.0 ± 0.2 keV, while the west lobe is slightly softer with values of 0.2 and 0.7 keV.

There are 364 total net counts in the lobes. Their total luminosity is 1.3×10^{40} erg s^{-1} , a result which is insensitive to the assumed spectral fit parameters (but see below). We fixed the absorption at the galactic value of 4×10^{20} cm^{-2} ; we were not able to obtain an acceptable fit with a single Raymond-Smith plasma for either lobe, but the sum of two temperatures was adequate (although of no physical significance with this small number of counts).

We note that ACIS-S is not very sensitive to diffuse hard emission. The hard background in our data gives a weak upper limit of about 1×10^{40} erg s⁻¹ for the 2-10 keV luminosity in the lobes, comparable to the observed soft luminosity. Therefore, although we have demonstrated the presence of low temperature X-ray gas in the lobes, we cannot rule out the presence of hotter temperature gas. Nevertheless, we see no evidence for the 1×10^{41} erg s⁻¹ of emission reported by Iwasawa et al (2001) from BeppoSAX data. This emission was detected in a 3 arcminute circle and is not inconsistent with our upper limit on this scale, but we can rule out its association with the inner regions of Arp 220; possibly they underestimated the contribution from Heckman’s group (see below). The spectra of the lobes and the plumes are compared in Fig. 7.

3.5. The background cluster

Fig. 8 shows a larger scale X-ray image which includes the region of Heckman et al.’s (1996) z=0.09 group 1RXH J153456.1+232822. The X-ray observations of this object and others in the field will be discussed in detail in Paper III (McDowell et al., in preparation). We briefly note here that we confirm the X-ray source as a diffuse object associated with the optical group and detect several embedded point sources. Galaxies Ohyama A and C (Ohyama et al. 1999, Grogin & Geller 2000), which are also 2MASS sources (2MASS, 1999), are both bright X-ray sources, with Ohyama A showing a soft extended plume, while the third cataloged galaxy, Ohyama B, is not detected. Two further bright point sources CXOU 153452.9+232833 and CXOU 153451.9+232828 are present within the cluster but have no counterparts on the POSS2 images.

4. Correspondence with other wavebands

4.1. Optical line emission

We obtained new integral field spectroscopy of the Arp 220 system in $H\alpha$ and NII as part of a program to study ionized gas in ULIRGs. Arribas, Colina & Clements (2001) presented observations of the nuclear region of the galaxy. The present observations were taken on 2000 May 8 and 9 on the 4.2m William Herschel Telescope using INTEGRAL (Arribas et al. 1998) and WYFFOS (Bingham et al. 1994) and consist of a mosaic of three pointings with a 30 arcsecond field-of-view fiber bundle.

As in other star forming galaxies studied by Chandra (e.g. Strickland et al 2000), there is a strong correlation of X-ray morphology with optical line emission. Heckman, Armus & Miley (1987) discovered the 20 kpc ‘double-bubble’ $H\alpha$ structure around Arp 220, as well as the inner $H\alpha$ SE plume.

The $H\alpha$ and soft X-ray morphology agree well in overall form and location - faint lobes, stronger plumes and the bright nuclear region - but there are differences in detail. Fig. 9 shows contours of $H\alpha$ emission superimposed on the soft X-ray image.

The peak of the $H\alpha$ emission coincides to within the 1" registration error with the soft X-ray peak (X-3). The holes in the lobes agree to within a couple of arcseconds, and the eastern plume is brighter than its western counterparts in both $H\alpha$ and X-rays. However, the brightest part of the line emission in the western lobe is shifted about 8 arcseconds south of the western X-ray lobe, and the eastern lobe is much more prominent in X-rays than it is in $H\alpha$. The peak of the SE plume is 2 arcseconds north of the plume’s soft X-ray peak.

For a typical electron density of 100cm^{-3} and temperature of 10^4 K we derive the mass of $H\alpha$ -emitting gas to be $2 \times 10^6 M_{\odot}$. The velocity in the plumes derived from the

H α observations (Colina et al 2003, in prep.) is about 200 km/s on average (with gradients up to 600 km/s in the lobes). Interpreting this as an outflow leads to a kinetic energy of 8×10^{53} erg s $^{-1}$.

4.2. Overall picture of Arp 220

Arp 220 is a complex system with tidal tails, dust lanes, and multiple nuclei. About 150 clusters and nine satellite galaxies can be seen on a recent HST I-band image (Paper III), reinforcing the impression that the Arp 220 system is massive compared to the Milky Way. The hard source X-1 is clearly associated with the galaxy’s central regions, and is probably coincident with the western nucleus Arp 220B (Paper I), although uncertainties in registration mean we cannot rule out an identification with the eastern nucleus. The soft emission and the X-3 peak (which also has a soft spectrum) coincide with the emission line peak rather than with the optical continuum peak. As other authors have discussed, the location of the optical peak is likely determined by gaps in the absorption and may not correspond to a physical object. None of the known optical and infrared clusters in this system (Shaya et al. 1994, Scoville et al. 1998) are detected in X-rays. X-2 is in a star cloud just to the south of the western end of the central dust lane; there is a probable cluster at 1.2 arcsecond from its estimated location, not close enough to propose as an identification.

The optical dust lane coincides with the separation between the nuclear emission and the SE plume, indicating that this separation is probably due to absorption. Interestingly, the plumes’ outer boundaries, while not sharp, coincide with a drop in the optical isophotes and plausibly represent the escape of the gas into a less dense halo interstellar medium. The axis of the plumes is perpendicular to the dust lane of Joy et al. (1986) and the CO disk, implying that they may be collimated in the inner region. One might expect the faintness of the NW plume to reflect its orientation deeper into the galaxy, but the X-ray spectrum

does not allow us to constrain the possibility of larger absorption in the NW. However, a second dust lane visible in the HST data bounds the brightest part of the NW plume on its northern side, implying that there may be more X-ray emission hidden behind it.

5. Discussion

5.1. The Superwind and the Plumes

Heckman et al. (1996) proposed that the extended H-alpha and soft X-ray emission in Arp 220 originates in a ‘superwind’ driven by starbursts which have been triggered by the merger. An alternate possibility, to be discussed in more detail by Hearn & Lamb (2003), is that the galaxy collision and merger dynamics are directly responsible for the extended structural morphology and hot gas. We consider each of these possibilities and conclude that both processes may play important roles in the Arp 220 system.

If Arp 220 is the product of the merger of two gas-rich disk galaxies, as is commonly thought to be the case because of the apparent presence of two, very close galactic nuclei and the overall disturbed morphology, then the physical processes that take place in this collision lead not only to conditions ripe for a central starburst, but also large-scale shocking of the interstellar gas over significant parts of the galactic disks. That is, in such a system, it is expected that a starburst-generated superwind will have to punch through a complicated region that lacks three dimensional symmetry, and consists of sectors of rapidly outflowing and inflowing shock-heated gas, coupled to sectors of flowing neutral gas that did not experience a direct impact. Thus the dominant flow direction of the superwind is likely to be constrained by the evolving geometry of the colliding system. The plumes will not expand into the regions of high pressure and high density, that comprise the hot expanding shocked gas and the cool expanding gas, respectively. The three dimensional morphology

of the overall system is very dependent on the collision parameters, and the time since first impact. Thus the environment of a superwind in a merging system is possibly different to that in a system like M82, that appears to be experiencing a central massive starburst in a previously relatively undisturbed disk galaxy.

Strickland and Stevens (2000) have used a combined Eulerian/Lagrangian hydrodynamics code to perform 2-D modeling of the superwind in M82, assuming cylindrical and reflection symmetry. As discussed by them, construction of a model to match the observed wind proved to be elusive, and will possibly require the inclusion of processes such as inflow of cold material or magnetic fields, to produce the observed confinement at the base of the wind in the starburst region. They conclude from their modeling that the bulk of the outflowing gas is at high temperatures of around $10^{7.5}\text{K}$ and low density, and would, therefore, be difficult to observe because of low emissivity. Interesting new information on the nature of starburst-driven winds and the interpretation of their observed X-ray fluxes is provided in Strickland et al. (2000). This tends to support the supposition that the temperature of the outflowing gas is not easily determined from X-ray data. They find that high-resolution Chandra observations of the kiloparsec-scale wind in NGC 253 demonstrate a strong correspondence between the X-ray and H-alpha observations of the outflow cone, with approximately equal amounts of energy being emitted from the hot gas in optical lines and in X-rays, and a total energy in both of the order of $10^{41} \text{ erg s}^{-1}$. This is about one percent of the mechanical energy estimated to be injected by the starburst. Strickland et al. (2000) also determined that the bulk of the X-ray flux originates in a limb-brightened structure, with at most 20% of the flux coming from the body of the fluid. This provides the first direct evidence that this radiation is generated at the interface between the outflowing gas and the ambient denser medium, rather than in the bulk of the flowing gas, whose temperature is, therefore, not well established.

Comparing our Chandra observations of Arp 220 with those of NGC 253, we see some similarities, despite the large difference in scale. As noted previously, the extended X-ray lobes in Arp 220 extend a distance of 10-15 kpc from the nucleus on the plane of the sky, and these also appear to be limb-brightened. The observed “edges” show reasonable overlap with the arcs of H-alpha emission in these regions, one each on the east and west sides (see Fig. 9). The lobes also display apparent central “holes” in the emission. In fact, the counts in the lobe regions are sufficiently low that our results are consistent with all of this soft X-ray flux originating within edge-brightened structures. However, although both sets of structures (plumes and lobes) appear to be produced by outflowing gas colliding with an external, denser medium, this may be an incorrect model for the lobes of Arp 220, because simulations of colliding galaxies indicate that the collision itself may have flung a dense ring-like structure of gas out on each side of the nucleus. For this system, we suggest that at these vast distances from the nucleus, it is the tidal interaction itself that is propelling the gas outwards; that there is shock heating within, and along the edges of the locally overdense structures, as demonstrated in previous studies of colliding galaxies (see Gerber et al, 1996, Lamb et al, 1998, and Hearn & Lamb, 2001); and that whether the source of the outflow energy is overpressure from a central starburst or tidally channeled galactic gravitational energy, the net effect is a strong correlation between the X-ray emission and H-alpha emission from gas that attains a temperature of around 10^6K in shocks at an interface.

The inner two plumes of hot gas observed in Arp 220 are likely to be due to a superwind that is driven by a central massive starburst, because such a wind would be a natural outcome (although similar features can be produced by flowing shocked regions of gas in slightly off-center galaxy collisions). In this first picture, the central regions have become sufficiently dense that a large fraction of the gas has cooled to form molecular gas and a super starburst has occurred. This latter has then produced a superwind which has

interacted with, and been somewhat channelled by the structures formed by the collision itself.

The extent of these plumes is large, spanning 11 kpc across the nuclear region. However, in contrast to the outflow cone in NGC 253, the Arp 220 plumes are very bright in soft X-rays, and no limb-brightening is noticeable in our data. The ambient medium into which these plumes are driving may be considerably different to that in NGC 253, consisting of entangled regions of shock-heated flowing gas and cooler, non-shocked gas, as discussed above. The energy flux coming from the central starburst in Arp 220 is larger than that from NGC 253 by a factor of 70, and this may also play a role in producing the different X-ray properties of the two objects. As noted in Section 3.3, the Chandra X-ray data for the Arp 220 plumes is consistent with a thermal plasma with temperatures ranging from 0.25 to 1 keV. This temperature range may result from the interaction of gas ejected in hot stellar winds and SN with regions of collisionally shock-heated gas, and with cooler flowing gas. That is, the entrained material may be of very varied initial temperature.

5.2. Merger Simulations

The overall context within which we wish to discuss our Chandra X-ray data for Arp 220 is that of a colliding pair of co-rotating, comparable mass, gas-rich galaxies which have not yet fully merged, but whose nuclei are now very close, and lie within a central disk of material that has been formed from remnants of the original two gaseous disks. Other disk remnants have been flung to large distances from the joint nuclear region. Relevant numerical modeling (Lamb et al 2003) indicates that the collision was likely almost face-on, and had an impact parameter of roughly 70% of the optical disk radius. Such a collision will leave some parts of the gas disks, those furthest from the impact point, unshocked by the direct collision, and this material is likely to retain its original temperature, whereas that

gas involved in the direct collision between the two disks will have been heated to over 10^6 K. All regions experience an initial inflow towards the impact point (that point in each disk where the center of mass of the other galaxy passes), followed by outflow, and then further inflow (see Gerber, Lamb, & Balsara, 1996). The subsequent, gravitationally-driven flows lead to relative gas velocities that are much larger in magnitude than the original impact velocity, with relative velocities of approximately 900 km/s obtained in some regions of the disk for the Arp 220 model fit, assuming that the Arp 220 system has a mass similar to that of the Milky Way. The rate of inflow and outflow in the disk material scales with the initial distance of the material from the impact point, being smaller for the more distant stars and gas. This, together with the asymmetries introduced by an off-center collision, lead to an evolving, intricate structure in the gas. As has been noted by many previous authors, such collisions can lead to the accumulation of large masses of gas in the merging nuclear region (for example, see Mihos and Hernquist, 1996). We note that this can only happen on a timescale of relevance to a system such as Arp 220 if the initial impact velocity is relatively low, less than a couple of a hundred km s^{-1} for galaxies with a mass of several $10^{11} M_{\odot}$, because larger impact velocities lead to a much longer merger time for the system as a whole.

The particular detailed numerical simulations of a pair of colliding gas-rich disk galaxies which was found to provide a suitable fit to the large-scale structure of Arp 220 was taken from a series of simulations in which mass ratio, impact velocity, impact parameter, relative disk spin direction, and relative tilt-angle of the two galaxies have been explored (Lamb et al., 2003). The 3-D simulations include a representation of the gas, stars, and dark matter, which all interact gravitationally. The gas hydrodynamics is followed using the method of Smooth Particle Hydrodynamics (SPH), and the gravitational potential is calculated on a grid for the full particle set. A description of the details of this n-body/SPH methodology, together with the galaxy starting models, is given in Gerber, Lamb & Balsara, 1996. We

note that in these simulations, the gas is considered to be isothermal. That is, there is no explicit heating and cooling in the simulation calculations. This is a useful approximation if one wishes to follow the overall dynamics of the gas and the build-up of dense regions, but we are not able to give a detailed map of the eventual temperature structure in the system. Rather, we can give a general description of the eventual location of that gas which has passed through shocks during the collision, and that gas which has not. An example of the latter is the gas that is in the outer edges of the disks that do not overlap at impact because of the off-center nature of the collision. This material is rapidly propelled outwards in the plane of the disks, after the brief overall contraction of the two galaxies.

A detailed exploration of the temperature distribution in the system as it evolves must await further modeling with appropriate physics included. However, it is of interest here to explore the range in possible post-shock temperatures obtained in the gas due to the collision. Assuming that the strong shocks that we have here are adiabatic, we can use the standard analytical expressions that relate the post-shock temperature of the gas T_2 to the relative velocity v of the colliding gas streams, and the adiabatic index γ and mean molecular weight μ of the gas (see Landau & Lifshitz 1987, Chapter 9). For a $\gamma = 5/3$ gas, $k_{\text{B}}T_2 = \mu \times v^2/3$. In the present situation, $\mu = 0.6m_{\text{H}}$, where m_{H} is the mass of the hydrogen atom. Thus for the maximum relative velocity found in our simulation of 900 km s^{-1} , we estimate the post-shock temperature is $\sim 2 \times 10^7 \text{ K}$. However, we expect the bulk of the shocked gas to be at a few million degrees because the relative velocities of the internally-generated gas streams range downwards from the maximum. For a relative velocity of 200 km s^{-1} , the post-shock temperature is just 10^6 K .

In Fig. 10, we present a view of the gas distribution in our best-fit 3-D model from a viewing angle appropriate to our line-of-sight to Arp 220. The gas density is represented by intensity (color in the electronic edition), as indicated in the figure caption. From an

inspection of the morphology of the simulation, we identify regions that correspond to the lobes and plumes observed in Arp 220, as shown in the figure. We also indicate the general regions in which mostly unshocked gas resides at this time in the evolution of the system. We connect these latter regions to those in Arp 220 that show HI emission, such as those observed by Hibbard, Vacca & Yun (2000).

The choice of model is constrained in both computational simulation epoch and in viewing angle. The distinct changes in the morphology of the simulated galaxies over relatively short time scales due to the collision dynamics produces the observed features only over a select range of times after the collision. There is some flexibility in the viewing angle chosen, but a very small fraction of the 4π steradians is available to produce a match. Projections of the complex three-dimensional structure of this collisional system onto the plane of the sky necessarily produces a wide range of distinct features that depend upon the direction from which the system is viewed. This restriction in viewing angle is a considerable strength of the model in that it places strong constraints on the predicted integrated line-of-sight velocities across the structure; these velocities can be compared to kinematic observations of Arp 220 when they are available.

We note that the simulations include the effects of gravity and gas dynamics on the preexisting stellar and gas distributions, but do not include the feed-back effects of star formation or a superwind on the gas dynamics. Nevertheless, the model shows that structures similar to those observed in Arp 220 can arise purely from the merger dynamics. We have demonstrated in previous studies (see Hearn & Lamb, 2001) that the dense regions that form in the gas due to a collision are prime sites of episodic, large-scale star formation events in colliding galaxies. Thus, we expect that star formation has taken place in the dense features that formed in Arp 220. Where young stellar populations have been formed, they will dominate the blue light, and will likely dominate the V-band also.

The maxima in the gas densities obtained in this simulation at this time in the outwardly propagating rings that form the outer edges of the "lobes" are approximately 2.2 and $2.4 \times 10^6 M_\odot \text{ kpc}^{-3}$ for the two respectively, again using Milky Way Galaxy scaling. The bulk of the material in these structures is at lower density, and $10^6 M_\odot \text{ kpc}^{-3}$ is a good average value. This is to be compared to a maximum in the inner regions of the model system of $3.8 \times 10^7 M_\odot \text{ kpc}^{-3}$ which occurs at a distance of about 3 kpc from the gravitational center at this epoch. All densities calculated in these simulations scale with the mass of the system.

The numerical models also provide a wealth of information on the velocity structure. However, the absolute values of the velocities and the time parameter in the simulations scale with the system mass and radius. In general, the computational units are chosen such that the quantity GMT^2/L^3 is a dimensionless scalar, where G is the gravitational constant, and T and L are the computational time and length units, respectively, and in these simulations, MT^2/L^3 is set equal to 1. Thus $T = L\sqrt{L/M}$, indicating that the gravitationally driven processes occur most rapidly in compact, massive galaxies. We do not have direct knowledge of the original radii of the two disk galaxies involved in the Arp 220 merger, nor do we yet have a very precise mass estimate for this system, therefore we will discuss the relative velocities generated in the model, and provide magnitudes based upon the mass and radius of the Milky Way galaxy for reference. We see from above that the scaling of the time unit is not very sensitive to the mass; we also note that the value of the length unit can be constrained by detailed comparisons of the models and observations of a particular system. In this case, the best fit model shown in Fig. 10 corresponds to a time 1.5×10^8 yr after the closest approach of the two nuclei, making Arp 220 a very young, incomplete merger.

These remarks should not be construed as implying that the full time interval of

approximately 1.5×10^8 years is available for a superwind to propagate out through the galaxy from the central nuclear region seen at this epoch in the model. Only after the joint nucleus is formed will enough stellar material be colocated over a long enough time to allow the enhanced star formation and merged superwind associated with a nuclear super-starburst. Although dense, presumably star-forming regions form in the gas in each disk very soon after the collision, their location in the disk changes over time, and none of these regions reform into the two galactic nuclei until well after the initial closest approach of the two nuclei. It takes an even longer time for the material from both disks to settle into one, joint central region, as observed in the Arp 220 system. The time for this central stellar turn-on is well defined in the sense that the central density remains low until this time and grows rapidly thereafter. In the chosen model, with the Milky Way scaling applied, the combined central region has been in existence for approximately 1.5×10^7 years, a factor of ten shorter than the time since the first closest approach. This then provides the timescale for the outward propagation of a superwind from a starburst in this central location. The central region will have been fed by a continual stream of infalling material during this 1.5×10^7 year period, which might be expected to help fuel an increasingly larger central starburst. This result is consistent with those of Mihos and Hernquist (1996) in their investigations of the timescale for central merger, infall of gas, and the potential production of a central starburst, in systems with somewhat different collision parameters than those presented here.

The regions in the model corresponding to the ‘plume regions’ in Arp 220 show an infalling of gas towards the nucleus of about 400 km s^{-1} , rather than the outflow of 225 km s^{-1} derived by Heckman et al (1996) for a superwind in this system. We note that both of these values would be reduced by projection effects as viewed on the sky and, at the approximate viewing angle given by our model fit, become approximately 300 km s^{-1} and 170 km s^{-1} , respectively. Neither of these numbers should be given great weight because

both are based on simple assumptions for the flow mechanism and the properties of the system. However, the interaction of an infalling collisionally shocked gas stream with a superwind would provide an interesting dynamical situation in the central regions of the galaxy and could lead to a slowed wind or to turbulent mixing, for example. In such a case the usual boundary conditions used in superwind calculations, such as those of Strickland & Stevens (2000) would need to be modified, and a 3-D simulation would likely be needed.

The outer, dense edges of the ‘lobe regions’ in the model are continuing to expand outwards and are experiencing a general rotation that is a remnant of the original rotation of the two disks. The rotational velocity is larger than that of the corresponding Keplerian velocity at that radius because a collision leads to an increase in the azimuthal velocity of the expanding ring (see Gerber 1993, and Gerber et al. 1996). The combination of the azimuthal and radial motions for these rings leads to a declining line-of-sight velocity along each of the lobe rims ranging from approximately 185 to 25 km s^{-1} , and -175 to -20 km s^{-1} , in the frame of the galaxy, for the two respectively. Insufficient observational data for these regions in Arp 220 currently exists to check these predictions against observations, but the detection of consistent rotation in the two lobe exteriors would provide support for our model.

Fig. 11 displays the distribution of the disk star particles corresponding to the same time step and viewing angle as shown for the gas distribution in Fig. 10. The particles representing the original disk stars are shown in black (yellow in the electronic version). We note that the distribution of the stars has an overall similarity to that of the gas, as both are driven primarily by the evolving gravitational potential. However, the density features in the gas are sharper than those in the stellar distribution because of the collisional nature of the gas, and the size of the expanding gaseous envelope is slightly smaller than the expanding remains of the stellar disk. In a real galaxy, we expect that the old original disk

stars would contribute heavily in the near-IR.

If we can assume that the original gas disks which formed Arp 220 did not extend far beyond their respective stellar disks, which is not a good assumption for all disk galaxies (see Briggs et al. 1980, Martin 1998), then we predict that the gas and the old, intermediate and low-mass stars should be found to roughly co-exist in space on large scales. That is, we expect the near IR flux from these stars in Arp 220 to extend as far as the X-ray and H-alpha images, or a little further. The collisional nature of the gas produces high density features not found in the stellar mass distribution, so the detailed structure is not the same in both, and the old stellar distribution in such systems can appear relatively smooth (see Stanford & Bushouse 1991) in comparison to that of the gas, and even more so in comparison to that of the new star-forming regions.

If either of the original disk galaxies had an extensive HI disk beyond the stellar disk, much of this material would now contribute to distended HI features on either side of the newly forming tight, central disk observed in the system. However, some fraction of the original HI gas, that residing on the near sides of the two disks during the collision, would have been collisionally shocked and heated to high temperatures. Galaxy collisions provide a means of heating large amounts of HI gas, as well as delivering vast amounts of material to the galaxy center, or into other dense regions, such as the extensive ring structures and tidal arms observed in some colliding systems (see Lamb, Hearn & Gao 1998, and Hearn et al. 2001), that can cool efficiently and subsequently form extranuclear superstarclusters. Indeed, Arp 220 does display such starclusters away from the nucleus, and the location and age of these can help to pin down the correct numerical models for this system, and even help to put constraints on the masses of the colliding galaxies.

5.3. The Lobes as Superwind or Merger Products

The lobes are morphologically distinct from the plume regions; their lower surface brightness and different position angle indicate that either the lobes and plumes are dynamically distinct, or that the outflowing material undergoes a transition at the lobe/plume boundary. In the latter case, we can interpret the lobes as the outflowing material from the plumes which has encountered a rapid drop in density at this radius in the galaxy’s halo and created a low-density, hot bubble of gas on either side of Arp 220. In principle, an unimpeded superwind of velocity $1000v_3$ km s⁻¹ could create a bubble of size $10r_{10}$ kpc in $1 \times 10^7(r_{10}/v_3)$ yr where r_{10} and v_3 are scaling parameters. This would be feasible, given the time scaling of our merger simulation, if we assume that we do not observe the lobes in projection, which would imply a larger true linear dimension, and that the central starburst occurred immediately after the combined stellar and gaseous nucleus formed. The numerical simulations indicate that the material now found in the central regions of Arp 220 was initially flung to a considerable distance from its current location, and has subsequently fallen back inwards in a steady stream that continues to this epoch. It appears unlikely that a strong, unimpeded superwind has existed for the last 10^7 yr. Further, if the true superwind velocity is low, as suggested by Arribas et al (2002), the timescale for lobe formation would be considerably longer than the maximum of 10^7 years available in the collision and merger model described here. If the true mass of the Arp 220 system is larger than that of the Milky Way, the time available for the superwind to propagate outwards is decreased.

In this section, we consider the alternative possibility that the connection between the lobes and the plumes is an artifact of projection and that the lobes arise purely from merger dynamics and collisional shock heating of the gas. As we mentioned earlier, the particular morphological form that appears to provide a good fit to the observed large-scale

structure of Arp 220 can be obtained for off-center, face-on, co-rotating disk collisions if the impact velocity is less than a couple of hundred km s^{-1} . If the impact velocity is larger, for example 300 km s^{-1} or more, lobes form and then disperse long before the nuclear region has had time to recondense, and we would not then expect either a starburst or its accompanying superwind to coexist with the collisionally induced lobes. The expanding, rotating, non-planar rings obtained in our chosen model, those that we identify with the outer, limb brightened portions of the lobes of Arp 220, do not appear ring-like from the chosen viewing angle. The gas contained within them was once a part of the two disks and has experienced both a collision with the gas from the other galaxy and, internally, with infalling, outer gas from the same disk. This latter process often leads to large-scale clumping of the gas, and a highly asymmetric density distribution around the ring (see Gerber, Lamb, & Balsara 1992), as well as very high relative velocities. In this picture, our line-of-sight to the centers of the lobes, as projected on the plane of the sky, passes through mostly very low density gas because the outwardly propagating ring structures have excavated these regions. The details of this proposed origin of the Arp 220 lobes can be further explored and checked against observations once detailed dynamical information for the lobes is available, and once a better mass estimate for the system is available from near-IR photometric imaging.

6. Conclusion

We have demonstrated the presence of distinct regimes in the X-ray emission in Arp 220: a nuclear region where a mixture of sources contribute (discussed in Paper I); a plume region of end-to-end dimension 11 kpc, with X-ray temperatures from 0.2 to several keV, that we suggest is likely associated with a superwind from the starburst at the center of the merger; two cooler diffuse lobe regions outside the optical galaxy with a temperature

of 0.2-1.0 keV, that stretch to 10-15 kpc on either side of the nuclear region. We suggest the lobes are a product of the collision itself, when a fraction of the gas gains a sufficiently higher than average share of the collision kinetic energy to radiate in the observed X-ray range. This picture helps to resolve several of the puzzles about this system raised by Heckman et al (1996); namely, the 'misalignment,' by 25-30 degrees, of the plumes and lobes, by attributing each to different structures rather than to a continuous structure, their apparent continuous appearance on the sky being caused by superposition; the integrity of the outer lobes, which we interpret as collisionally produced ring structures, rather than the outer edges of a wind-blown bubble which might be expected to have experienced 'blow-out' by this time; and the collimation of the supposed wind-blown plumes which may have been influenced by the collisionally modified phase and velocity structure of the near-disk galactic environment. We note that the disk itself is likely to have only recently reformed after the disk disruption caused by the initial collision of the galaxies.

Arp 220 is a prototype for the large number of rapidly star-forming infrared mergers at higher redshift. The complexity of its interstellar medium is a salutary warning of the difficulty of interpreting data with poorer linear resolution. If the Arp 220 X-ray lobes are due to a superwind, the amount of energy being pumped into the intergalactic medium is a significant fraction of the energy generated by the starburst, in contrast to that of the superwind of NGC 253 which has an energy of just a few percent of the output from the central starburst. If the lobes are a dynamical collision remnant, they may provide a source of infalling material at later times, but can also be dispersed into the intergalactic medium if the collision parameters and galactic environment are appropriate (Hearn & Lamb 2003).

We acknowledge use of the ADS, SIMBAD, NED, and CIAO.

Partial support for this work was provided by the National Aeronautics and Space Administration through Chandra Award Number GO1-1166 issued by the Chandra X-Ray

Observatory Center, which is operated by the Smithsonian Astrophysical Observatory for and on behalf of NASA under contract NAS8-39073. S. Lamb and N. Hearn acknowledge support from DOE contract LLNL B209032 and the support of NPACI through an allocation of computer time to perform the numerical simulations presented in this paper, and to NSCA for computational support for visualization of the models. We thank the referee for helping us clarify the presentation.

REFERENCES

- Arp, H.C., 1966, ApJS 14, 1.
- Armus, L., Shupe, D.L., Mathews K, Soifer, B.T., & Neugebauer G., 1995, ApJ 440, 200.
- Arribas, S., et al. 1998, SPIE 3355, 821.
- Arribas, S, Colina, L., & Clements, D.L., 2001, ApJ 560, 160.
- Baan, W.A., Wood, P.A.D & Haschick, A.D., 1982. ApJ 260L, 49.
- Bingham, R., et al. 1994, SPIE 2198, 56.
- Briggs, F.H., Wolfe, A.M., Krumm, N., & Salpeter E.E., 1980, ApJ 238, 510.
- Chevalier, R.A., & Clegg, A.W., 1985, Nature 317, 44.
- Clements, D.L., et al. 1996, MNRAS, 279, 477.
- Clements, D.L., et al. 2002 (Paper I), ApJ, submitted.
- Colina, L, et. al, 2003, in preparation.
- Dreyer, J.L.E., 1910, Mem. RAS, 59, 105.
- Dudley, C.C, & Wynn-Williams, C.G 1997, ApJ 488, 720.
- Eales, S.A., & Arnaud, K.A., 1988, ApJ 324, 193.
- Gallagher, S.C., et al 2002, ApJ 569, 655.
- Genzel, R., et al. 1998, ApJ 498, 579
- Gerber, R.A., 1993, Ph.D. thesis, University of Illinois.
- Gerber, R.A., Lamb, S.A., & Balsara D.S., 1992, ApJ 399, L51.
- Gerber, R.A., Lamb., S.A., & Balsara, D.S., 1996, MNRAS 278, 345.
- Grogin, N.A., & Geller, M.J, 2000, AJ 119, 32.
- Hearn, N.C., & Lamb, S.A., 2001, ApJ 551, 651.

- Hearn, N.C., & Lamb, S.A., 2003, in preparation.
- Heckman, T.M., Armus, L., & Miley, G.K., 1987, AJ 92, 276.
- Heckman, T.M., Dahlem, M., Eales, S.A., Fabbiano, G., & Weaver, K., 1996, ApJ 457, 616.
- Hibbard, J.E., Vacca, & Yun 2000, AJ 119, 1130.
- Iwasawa, K. Matt, G., Guainazzi, M., & Fabian, A.C., 2001, MNRAS 326, 894.
- Javelle, 1905, Observatoire de Nice, Annales, T. xi., D.1.
- Joy, M., Lester D.F., Harvey P.M., & Frueh M., 1986, ApJ 307, 110.
- Kim, D-C. & Sanders, D.B. 1998, ApJS 119, 41.
- Lamb, S.A., Hearn, N.C., & Gao Y., 1998, ApJ 499, L153.
- Lamb, S.A., Hearn, N.C., Morgan, J.C., Kwon, S., & Gerber, R.A., 2003, in preparation.
- Landau, L. D. & Lifshitz, E. M. 1987, *Fluid Mechanics, Second Edition*, Butterworth-Heinemann, Oxford
- Lonsdale, C.J, Diamond, P.J. & Smith, H.E., 1994, Nature 370, 117.
- Lutz, D., et al. 1998, ApJ 505, L103.
- Ohyama, Y., Taniguchi, Y., Hibbard, J.E., & Vacca, W.D, 1999, AJ 117, 2617.
- Markevitch, M., et al. 2000, ApJ 541, 542.
- Martin, M.C., 1998, A&AS 131, 73.
- Mihos, J.C. & Hernquist, L., 1996, ApJ 464, 641.
- Rieke, G.H., et al. 1985, ApJ 290, 116.
- Safford, T.H., 1887, Annual Rep. of the Board, Chicago Astronomical Society, 1885-1886,
Appendix C.
- Scoville, N.Z., et al. 1998, ApJ 492, L107.

Shaya, E.J, et al., 1994, AJ 107, 1675.

Soifer, B.T. et al. 1984, ApJ 283, L1.

Stanford, S.A., & Bushouse, H.A., ApJ 371, 92.

Stark, A., et al 1992, ApJS 79, 77.

Strickland, D. K., Heckman, T.M., Weaver, K.A, & Dahlem M, 2000, ApJ 120, 2695.

Strickland, D.K., & Stevens IR, 2000, MNRAS 314 511

2MASS Team, 1999, The 2MASS Spring99 Release Extended Source Catalog.

Table 1: Flux of Arp 220 X-ray Components

Object	Position (J2000)	PA ^a	Extent ($''$)	Net counts	F_{14}^b (obs)	L_{40}^c (obs.)	L_{40}^d (corr)	$\log L(\text{H}\alpha)^e$ (erg s^{-1})
Arp 220 Circumnuclear	15:34:57.14 +23:30:13.0	-	7 $''$	250	1.6	1.1	6	39.8
Arp 220 X-1 hard halo ^f	15:34:57.28 +23:30:11.4	-	3 $''$	113	5.9	4.1	8?)
Arp 220 X-1 (nucleus) ^f	15:34:57.21 +23:30:11.7	-	Unres.	66	3.0	2.1	4?) 39.9
Arp 220 X-4 ^f	15:34:57.25 +23:30:11.5	-	Unres.	19	1.0	0.7	1.5)
Arp 220 X-2 ^f	15:34:56.94 +23:30:05.5	-	Unres.	33	1.0	0.6	0.7	<38.0
Arp 220 X-3	15:34:57.14 +23:30:13.1	-	2 $''$	31	0.2	0.1	0.6	39.7
Arp 220 SE Plume	15:34:57.64 +23:30:06.0	135	7 $''$ x 14 $''$	409	3.3	2.3	>2.5	40.2
Arp 220 NW Plume	15:34:56.96 +23:30:17.4	331	8 $''$ x 9 $''$	135	0.8	0.5	>0.7	39.6
Arp 220 E Lobe	15:34:59.21 +23:30:02.6	111	23 $''$ x 15 $''$	188	0.9	0.6	0.7	39.3
Arp 220 W Lobe	15:34:55.58 +23:30:14.0	280?	10 $''$ x 22 $''$	176	1.0	0.7	0.8	39.6
Arp 220 remainder				274	1.5	1.0	1.2	40.0
Arp 220 total				1694	20.2	13.8	>26	40.7

^a Position angle in degrees of the line joining the feature to the nucleus.

^b Observed flux in the 0.3-10.0 keV band in units of $10^{-14} \text{erg cm}^{-2} \text{s}^{-1}$.

^c Luminosity corresponding to observed flux in units of $10^{40} \text{erg s}^{-1}$ (uncorrected for absorption).

^d Luminosity corrected for X-ray absorption, in the same units.

^e Log of H α luminosity (Colina et al in prep.)

^f These are the only components with significant flux detected above 2 keV. Observed soft flux for these components totals $4 \times 10^{39} \text{erg s}^{-1}$.

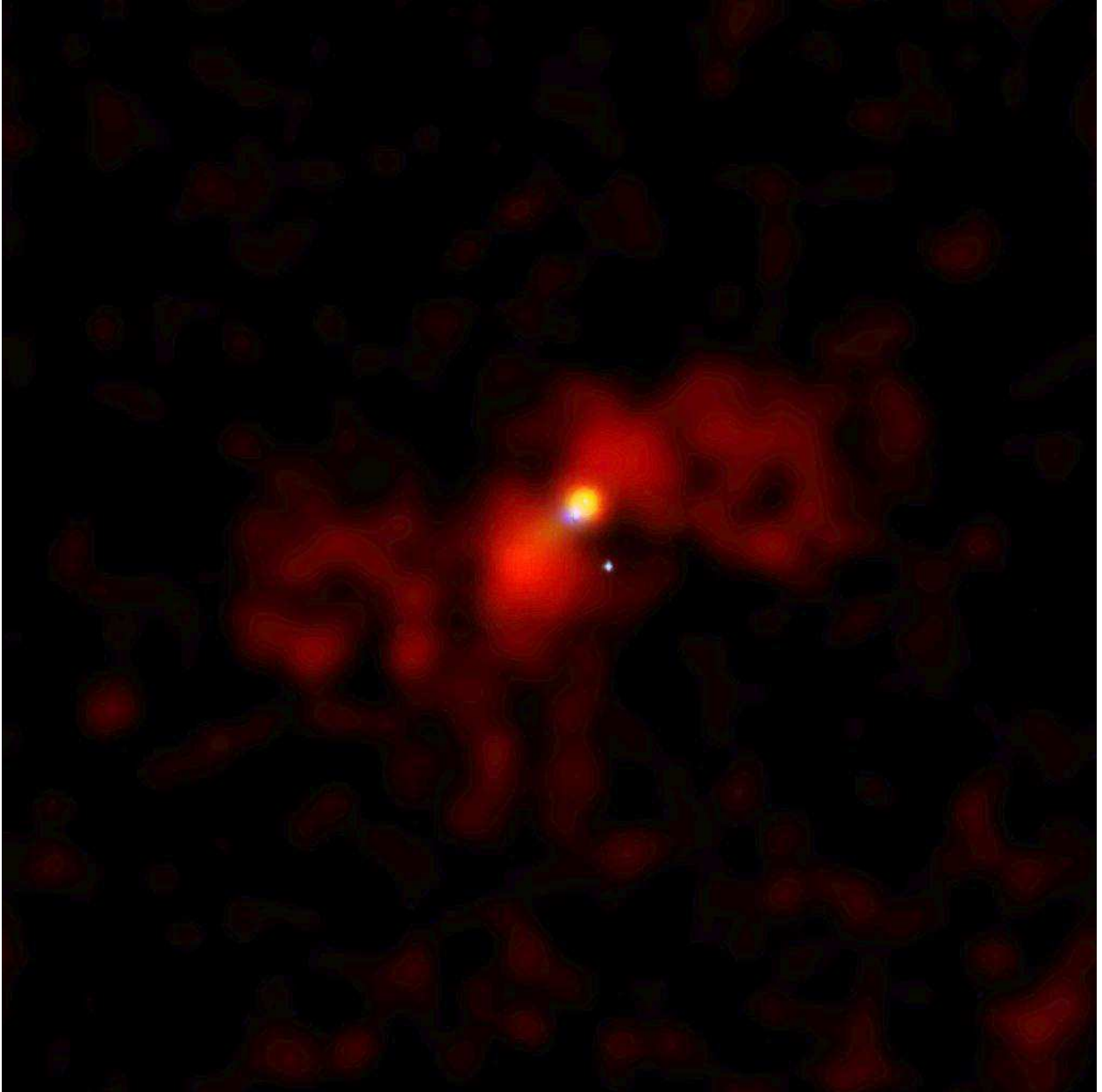


Fig. 1.— Adaptively smoothed true X-ray color image of Arp 220. Red represents the 0.2-1.0 keV band, green the 1.0-2.0 keV band, and blue the 2.0-10.0 keV band. Field shown is 2.1' square.

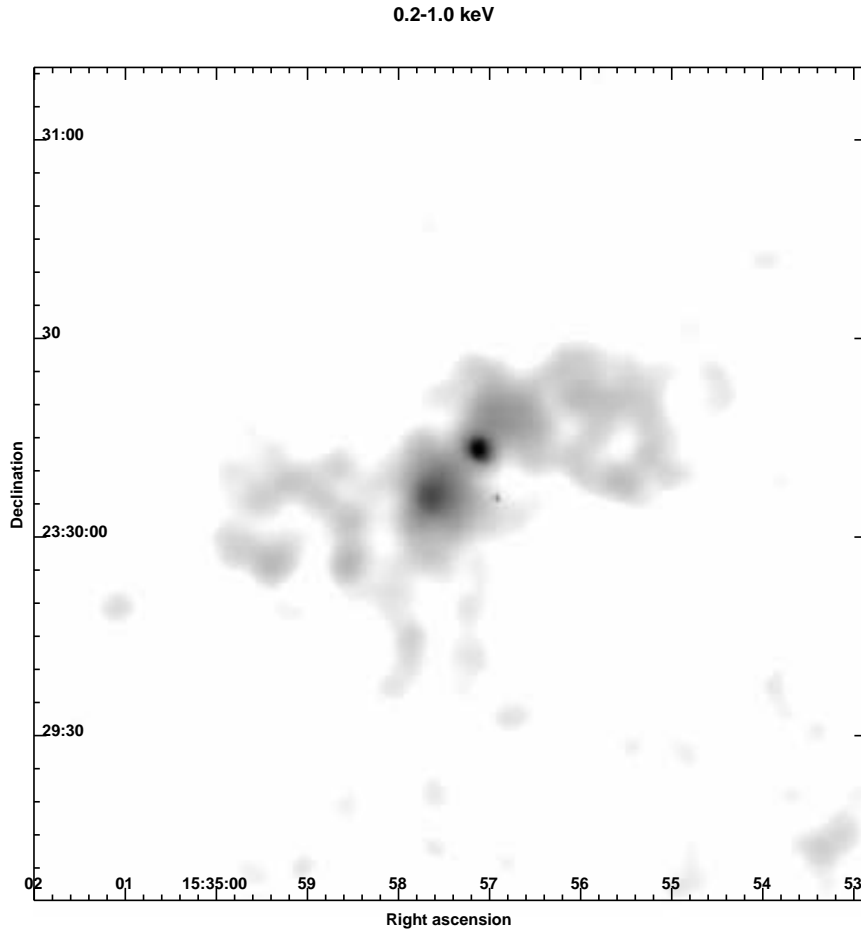


Fig. 2.— Adaptively smoothed images of the Arp 220 region in three bands: (a) 0.2-1 keV

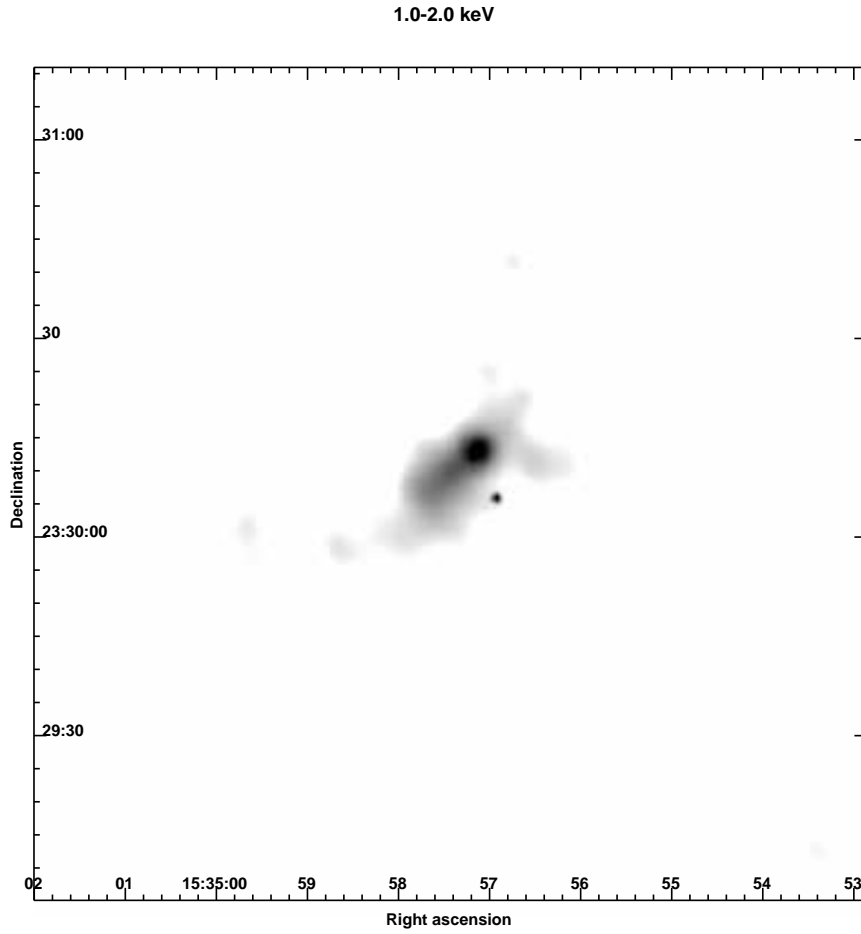


Fig. 3.— Adaptively smoothed images of the Arp 220 region in three bands: (b) 1-2 keV.

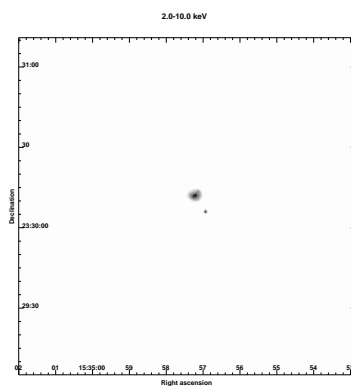


Fig. 4.— Adaptively smoothed images of the Arp 220 region in three bands: (c) 2-10 keV.

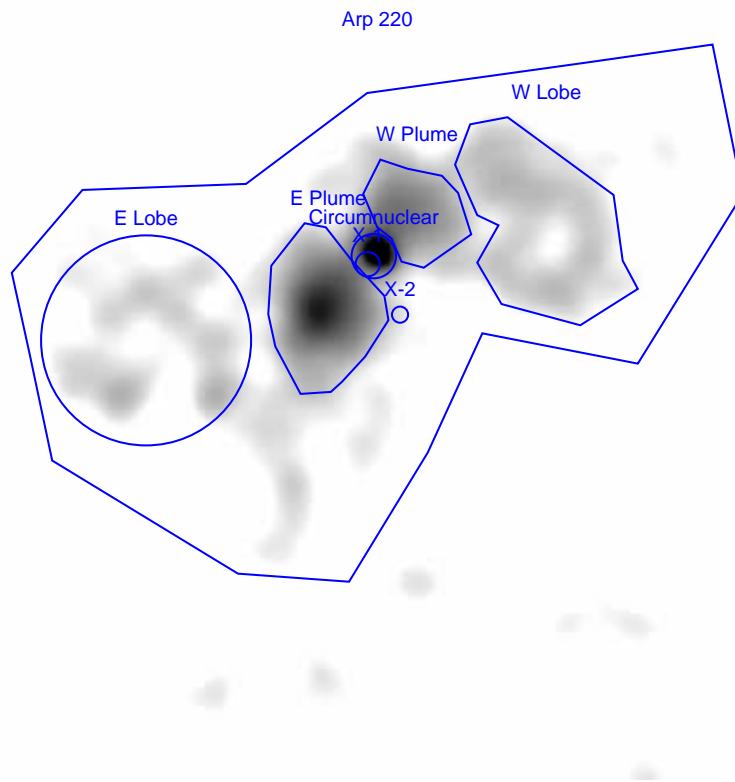


Fig. 5.— Extraction regions used for spectral analysis, overlaid on smoothed soft band image.

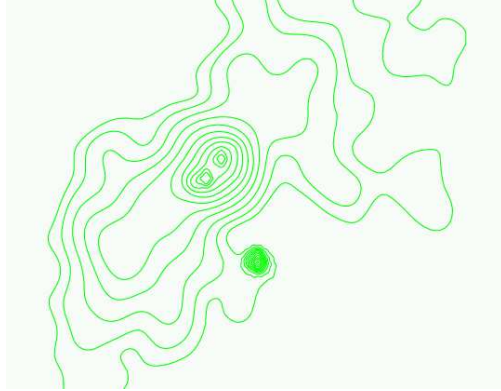


Fig. 6.— Reconstructed image of central part of Arp 220, showing plumes and circumnuclear region in the 0.2-10.0 keV band. In each of the three energy bands, the three point sources X-1, X-2 and X-3 were subtracted, the remaining emission was adaptively smoothed, and then PSFs for the three sources were added back in. The southeast ‘nucleus’ is X-1 and the northwest ‘nucleus’ is the soft peak X-3; X-2 is the strong peak to lower right of image. Intensity contours are logarithmically spaced 0.2 dex apart.

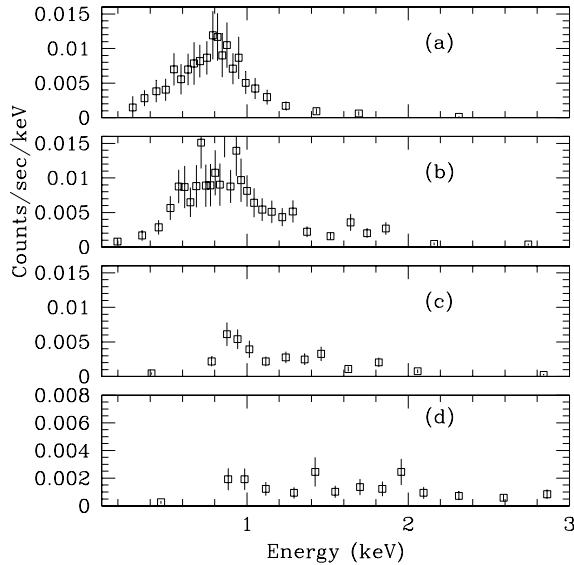


Fig. 7.— Background-subtracted pulse height (PI) spectra for (a) the lobes, (b) the plumes, (c) the circumnuclear region and source X-3, and (d) the X-1 region.

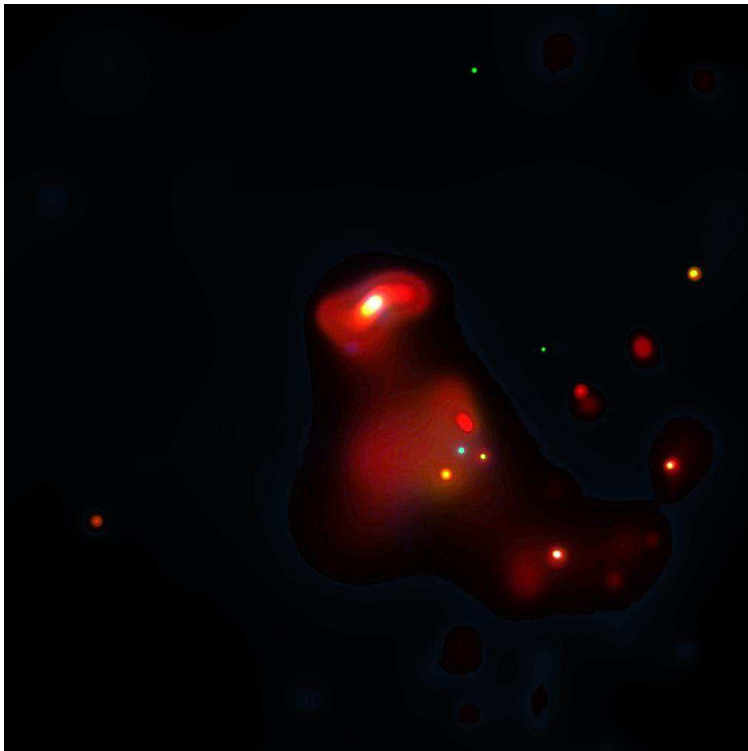


Fig. 8.— The Arp 220 field (0.2-10.0 keV), adaptively smoothed to bring out emission from the cluster.

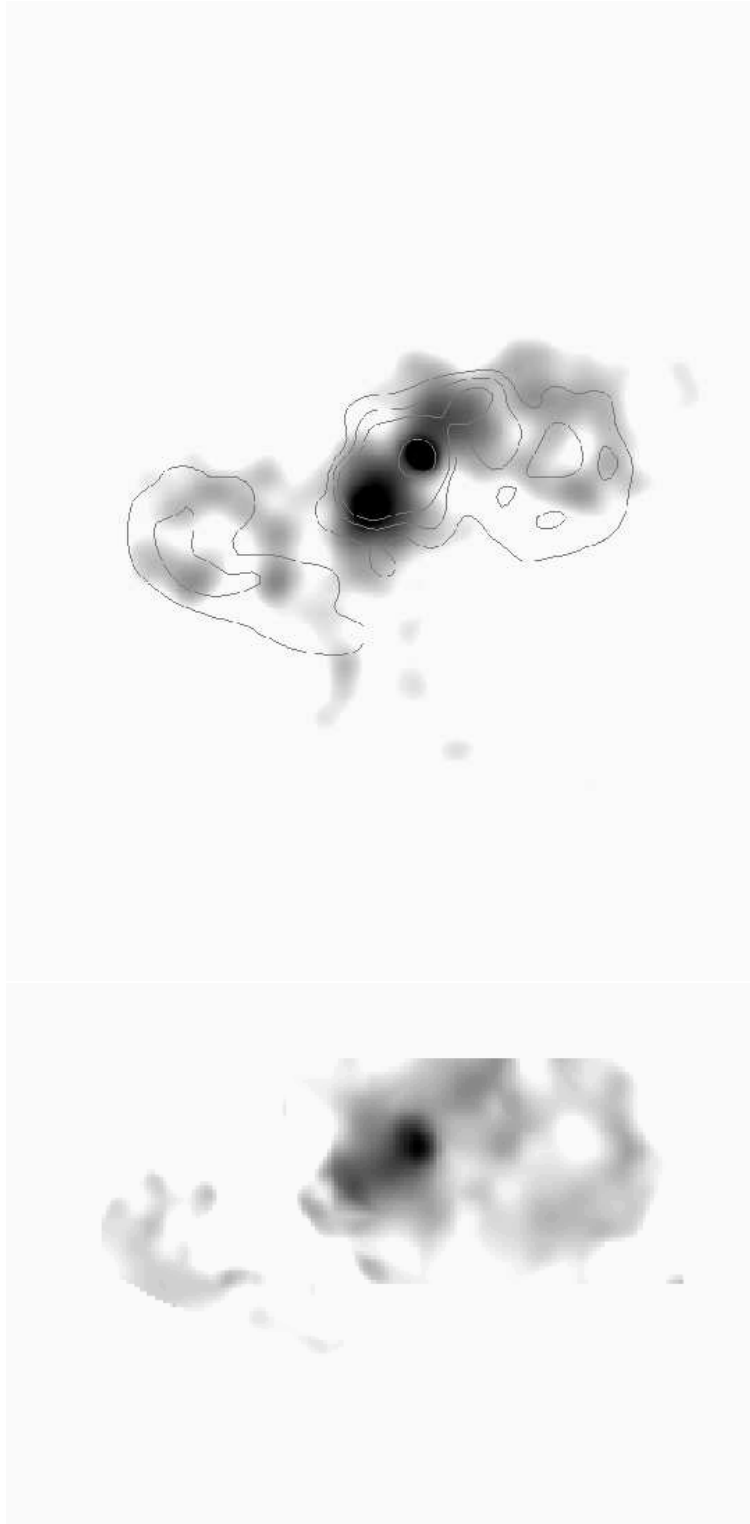


Fig. 9.— Top: H-alpha contours overlaid on the soft X-ray greyscale. Bottom: H-alpha greyscale; field of view is cut off at north boundary. Data from Colina et al. (2003).

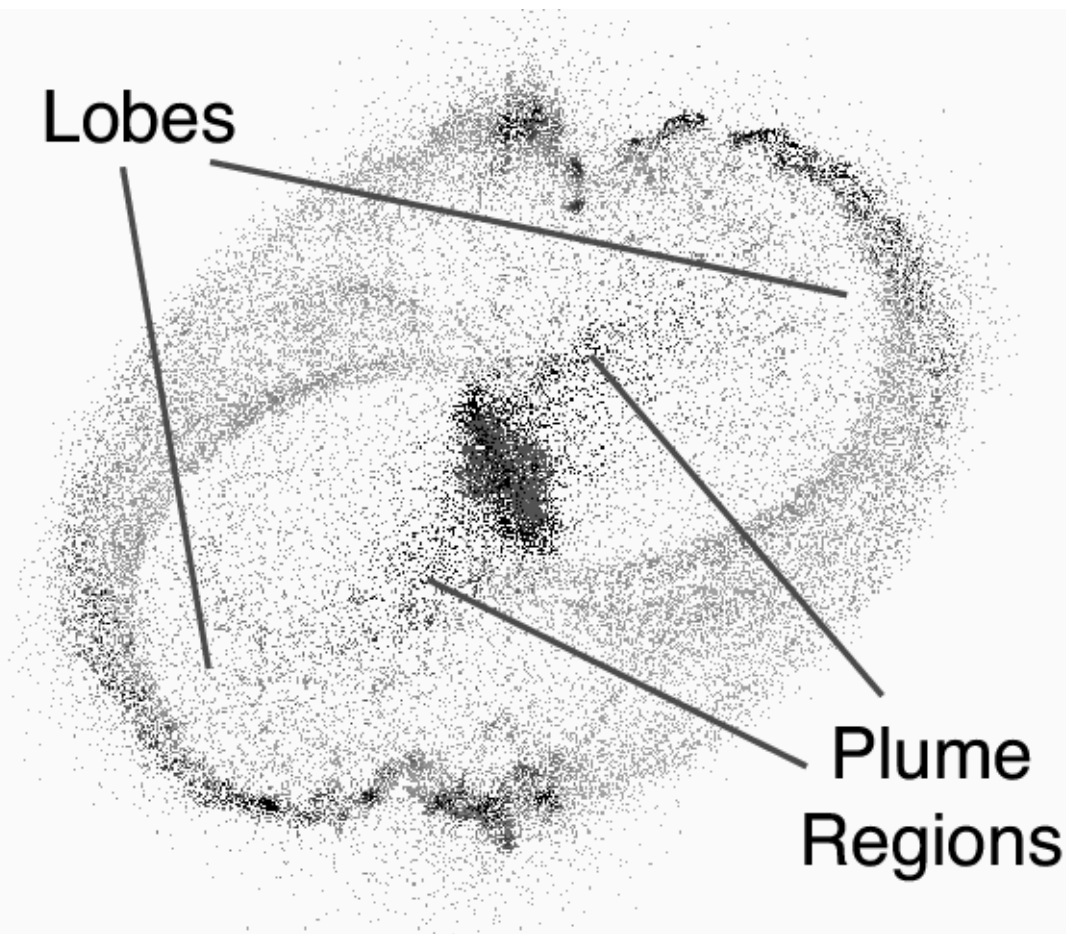


Fig. 10.— Dynamical simulation of the Arp 220 merger. Image shows the gas density distribution at a time of 1.5×10^8 yr after closest approach and 1.5×10^7 yr after the formation of the dense central stellar region. Density is indicated by intensity in the paper version, and by color in the electronic version (red represents the densest gas and blue the least dense). The system is viewed from an angle chosen to match the Arp 220 observations. The regions corresponding to the lobes and the plumes are indicated. The entire gaseous component is shown here, which includes the hot gas seen in the X-ray observations, as well as the cool, neutral gas observed in H I. The lobe regions are bounded by the arcs of relatively dense gas to the far left and far right edges of the distribution. Much of the gas interior to these arcs is falling back toward the nuclear region after having been flung to large distances during the collision. The arcs themselves are the remains of large density perturbations triggered by the collision dynamics, and are the sites of strong shocks. Material falling into the lobe regions from these arcs would have been heated by the large-scale shock waves. The infalling material includes the central plume-like regions along the lower-left to upper-right diagonal; this gas could be countered by strong outflows from a central starburst in the real system. Outside of the lobes, low density gas can be found along the upper-left to lower-right

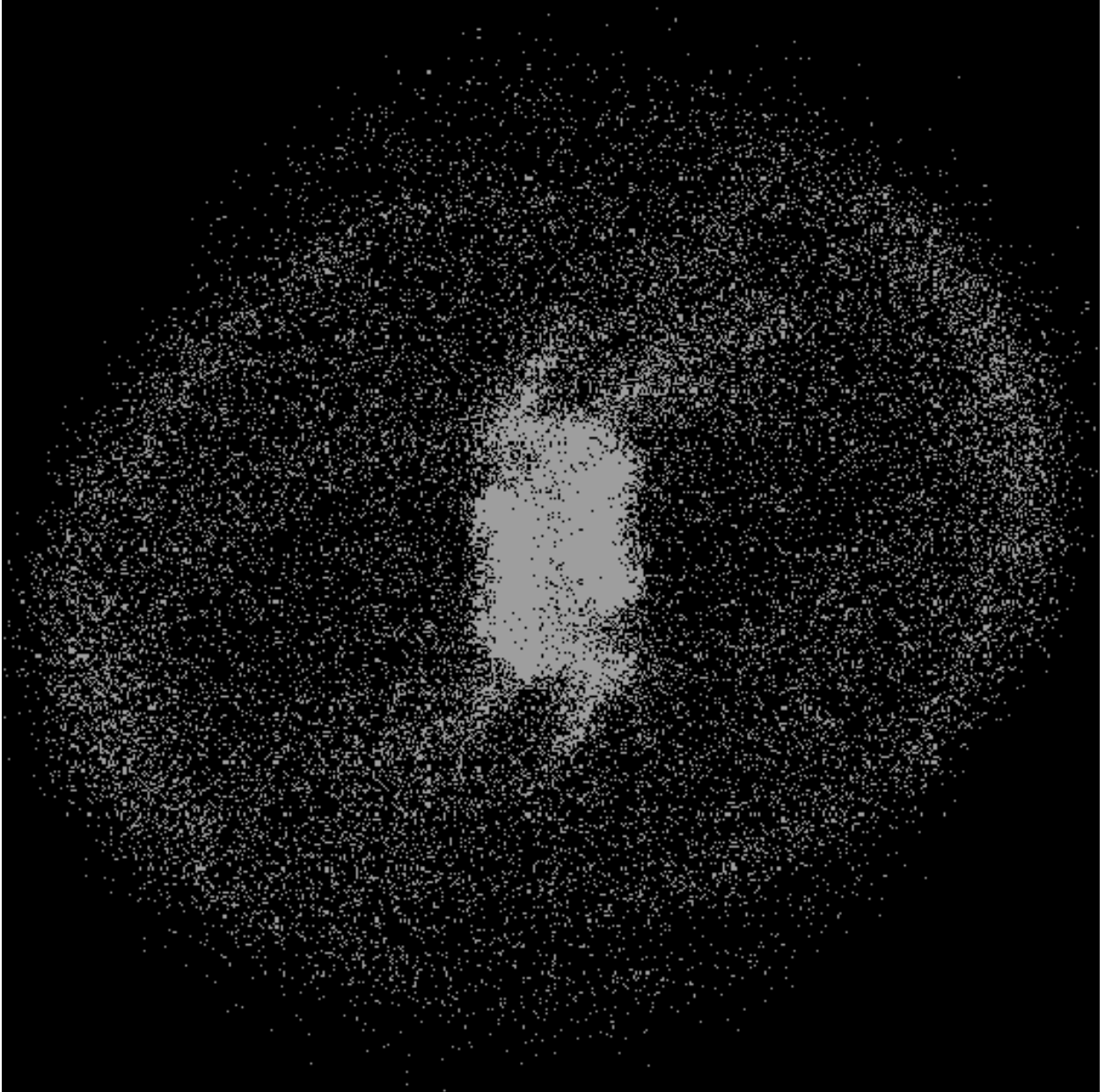


Fig. 11.— Dynamical simulation of the Arp 220 merger. Image shows the total star density distribution; details as for Fig. 10.